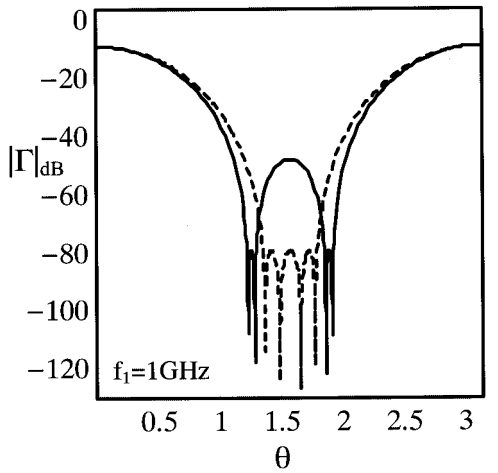


**Figure 7** Absolute reflection coefficient vs. $\theta$ for DBCT (solid) and SBCT (dashed) with the same passband tolerance $\rho_m$ ($f_2/f_1 = 1.5$, $\Delta f/f_2 = 0.02$)

SBCT does not cover both required bandwidths for all the cases discussed above.

#### 4. CONCLUSION

We have introduced a new dual-band multisection transformer based on a straightforward generalisation of the standard (small-reflection) Chebyshev synthesis. The proposed method, in the present form, applies whenever the upper-band centre frequency $f_2$ is less than three times the lower-band centre frequency $f_1$, and the (absolute) bandwidths are the same $\Delta f$. For given centre frequencies $f_1$, $f_2$ and bandwidth $\Delta f$, the proposed design is definitely better than the classical single-band Chebyshev transformer with passband $f_1 - \Delta f$, $f_2 + \Delta f$, in terms of passband tolerance, and hence the larger the difference $f_2 - f_1$ and the smaller the (fractional) bandwidth $\Delta f/f_2$. This method can be more or less obviously generalised to multiband transformers with different (absolute) bandwidths.

#### APPENDIX

The trigonometric Chebyshev polynomial $T_M(a\cos^2\theta + b)$ can be expressed for $M = 1, 2, 3, 4$ as

$$T_1(a\cos^2\theta + b) = \frac{1}{2}(a + 2b + a\cos 2\theta), \tag{A1}$$

$$T_2(a\cos^2\theta + b) = \frac{1}{4}[-4 + 3a^2 + 8ab + 8b^2 + 4a(a + 2b)\cos\theta + a^2\cos 4\theta], \tag{A2}$$

$$T_3(a\cos^2\theta + b) = \frac{1}{8}[-12a + 10a^3 - 24b + 36a^2b + 48ab^2 + 32b^3 + 3a(-4 + 5a^2 + 16ab + 16b^2)\cos 2\theta + 6a^2(a + 2b)\cos 4\theta + a^3\cos 6\theta], \tag{A3}$$

$$T_4(a\cos^2\theta + b) = 1 - 3a^2 + \frac{35a^4}{16} - 8ab + 10a^3b - 8b^2 + 18a^2b^2 + 16ab^3 + 8b^4 + \frac{1}{2}a(-8a + 7a^3 - 16b + 30a^2b + 48ab^2 + 32b^3)\cos 2\theta + \frac{1}{4}a^2(-4 + 7a^2 + 24ab + 24b^2) \times \cos 4\theta + \frac{1}{2}a^3(a + 2b)\cos 6\theta + \frac{1}{16}a^4\cos 8\theta. \tag{A4}$$

The above formulae are readily generalised to any order, by using the Chebyshev polynomial recurrence formulae in [8] and the expansions of $\cos^n\theta$ in terms of $\cos(m\theta)$, $m = 0, \ldots, n$.

#### REFERENCES


1. R.E. Collin, Foundations for microwave engineering, 2nd ed., McGraw-Hill, New York, 1992, Ch. 5.
2. D.M. Pozar, Microwave engineering, 2nd ed., Wiley, New York, 1998, Ch. 5.
3. Y.L. Chow and K.L. Wan, A transformer of one-third wavelength in two sections—for a frequency and its first harmonic, IEEE Microwave Wireless Compon Lett 12 (2002), 22–23.
4. V.P. Meschanov, I.A. Rasukova, and V.D. Tupikin, Stepped transformers on TEM transmission lines, IEEE Trans Microwave Theory Tech 44 (1996), 793–798.
5. S.B. Cohn, Optimum design of stepped transmission line transformers, IRE Trans Microwave Theory Tech 3 (1955), 16–21.
6. R.E. Collin, Theory and design of wide band multisectional quarter wave transformer, Proc IRE 43 (1955), 179–185.
7. H.J. Riblet, General synthesis of quarter wave impedance transformer, IRE Trans Microwave Theory Tech 5 (1957), 36–43.
8. M. Abramowitz and I.E. Stegun, Handbook of mathematical functions, Dover, Mineola, NY, 1972.




## ELECTRICAL AND OPTICAL PROPERTIES OF $CaCu_3Ti_4O_{12}$ (CCTO) SUBSTRATES FOR MICROWAVE DEVICES AND ANTENNAS


**L. C. Kretly,[1] A. F. L. Almeida,[2] R. S. de Oliveira,[3] J. M. Sasaki,[4] and A. S. B. Sombra[5]**

[1] Departamento de Microondas e Óptica (DMO)
Faculdade de Engenharia Elétrica e Computação (FEEC)
UNICAMP
[2] Departamento de Química Orgânica e Inorgânica
Centro de Ciências, UFC
Fortaleza, Ceará, Brazil
[3] Departamento de Física
Universidade Estadual do Ceará (UECE)
Fortaleza, Ceará, Brazil
[4] Laboratório de Raios-X
DF-UFC
UNICAMP
[5] Laboratório de Óptica Não Linear e Ciência e Engenharia dos Materiais (LOCEM)
Departamento de Física, UFC
Campus do Pici, Caixa Postal 6030-CEP 60.455-760
Fortaleza CE, Brazil


*Received 23 June 2003*

**ABSTRACT:** *The solid-state procedure is used to produce bulk ceramics of CCTO ($CaCu_3Ti_4O_{12}$). The samples of the CCTO ceramic are studied by X-ray powder diffraction and infrared and Raman scattering spectroscopy. The infrared and Raman scattering spectroscopy confirm the formation of the CCTO phase, as seen by X-ray diffraction (XRD) analysis. One experimental procedure uses an organic binder in the process of shaping the samples. In the second procedure, the samples were prepared without the presence of the organic phase, and we ob-*

*tained a higher dielectric constant (K = 7370) with higher loss (D = 0.2) at 1 KHz. For the first procedure, a lower dielectric constant (K = 1530) and lower loss (D = 0.11) at 1 KHz were obtained. Simple rectangular antenna prototypes were also designed on substrate samples (C1, C2, P1, and P2). For the antennas with P2, C1, and C2 as substrates, the bandwidth (BW) is 90 MHz (around 3%). The antenna with P1 substrate presents a surprisingly high BW of 270 MHz, which corresponds to a 10% bandwidth. Such a value is in accordance with the requirements for planar antennas in a variety of wireless communication systems such as WLAN, PCS, Wi-Fi, and other protocols. Therefore, these measurements confirm the potential use of such materials for small high-dielectric planar antennas (HDAs). These materials are also attractive for capacitor applications as well as for microelectronics and microwave devices (cellular mobile phones, for example), where miniaturization of the devices is crucial.* 
Microwave Opt Technol Lett 39: 145–150, 2003; Published online in Wiley InterScience (www.interscience.wiley.com). DOI 10.1002/mop.11152

**Key words:** *miniaturized microwave devices; CCTO substrate materials; miniaturized antennas*

## 1. INTRODUCTION

High dielectric constants have been found in oxides of the type $CaCu_3Ti_4O_{12}$ (CCTO) [1–3], which show a dielectric constant at 1 KHz of about 10.000, which is nearly constant from room temperature to 300°C. Oxides with the perovskite structure are well stabilised by their high dielectric constants (DC), which lends these class of materials to a large number of technological applications [4]. However, this behaviour is generally associated to ferroelectric or relaxor properties. In these cases, the highest value of the DC is obtained during a phase transition (as a function of temperature) presented by the material.

The existence of the transition temperature event is generally a problem regarding applications of these materials. The reported results for CCTO show that the DC is high, but has small dependence on the temperature [3].

Such material is very promising for capacitor applications and certainly for microelectronics and microwave devices (cellular mobile phones, for example), where miniaturization of the devices are crucial.

High DC ceramics make it possible to noticeably miniaturize passive microwave devices. Their size can typically be reduced in comparison with classical resonators and filters by a factor of $\sqrt{\varepsilon_r}$ (relative dielectric constant).

The structure of CCTO was previously determined from neutron powder diffraction data [5], and belongs to space group Im3 (No. 204) [5]. Recently, we proposed the use of a mechanical alloying technique to produce CCTO [6]. Mechanical alloying is proving to be a powerful method to obtain any quantity of powder with a controlled microstructure [7]. Recently, a polymeric-citrate precursor route was used to produce CCTO [8]. A dielectric constant of 3.000 and loss around 0.3 to 0.35 at 1 KHz were observed.

In this work, we report on the preparation of the ceramic of CCTO through the solid-state route and use the bulk ceramic as a substrate for a planar microwave antenna application. The produced samples were studied using X-ray diffraction (XRD) and infrared and Raman Spectroscopy techniques. The dielectric constant and loss were also studied in the range of 100 Hz to 1 MHz.

The production and the study of the properties of CCTO ceramics is important in view of possible applications as bulk devices, such as microwave resonators and oscillators, and thick and thin high-DC films.

**TABLE 1 Sample Properties**

| Sample CCTO(CS) | Thickness $e$ (mm) | Electrode diameter $L$ (cm) | Dielectric Loss (D) · $10^{-2}$, $D = \varepsilon''/\varepsilon'$ 1 KHz and 1 MHz | Dielectric Constant $K = \varepsilon'/\varepsilon_0$ 1 KHz 1 MHz |
|---|---|---|---|---|
| C1 | 2.61 | 4.7 | 11 | 1530 |
| | | | 35 | 718 |
| C2 | 2.29 | 4.7 | 11 | 1641 |
| | | | 37 | 769 |
| P1 | 2.12 | 3.6 | 20 | 7370 |
| | | | 34 | 4271 |
| P2 | 2.12 | 4.2 | 22 | 7073 |
| | | | 61 | 3444 |

All samples are CCTO(CS). Samples C1 and C2 were prepared with an organic binder. Samples P1 and P2 were prepared without any organic phase. All the samples were submitted to calcination (C) and sintering (S).

## 2. EXPERIMENTAL PROCEDURE

### 2.1. Sample Preparation

Commercial oxides $Ca(OH)_2$ (Vetec, 97% with 3% of $CaCO_3$), titanium oxide ($TiO_2$) (Aldrich, 99%), CuO (Aldrich, 99%) were used in the CCTO preparation. The material was ground on a Fritsch Pulverisette 6 planetary mill with a proportionality of $Ca(OH)_2$—3CuO—$4TiO_2$. Milling was performed in sealed stainless steel vials and balls under air. Mechanical alloying was performed for 1 h of milling. In this case, the milling was used only to provide the powder with good homogeneity. However, we had previously found that for 100 h of milling the complete production of CCTO is possible [6]. The reaction that occurs during milling can be summarised as:

$$Ca(OH)_2 + 3CuO + 4TiO_2 \xrightarrow{\text{IMPACTS}} CaCu_3Ti_4O_{12} + H_2O.$$

The powder was mixed with an organic binder and compacted into disks at a pressure of 2.5 tons. The pellets were then sintered at 1050°C for 24 h. These samples were denominated by C1 and C2 (see Table 1). The same powder was prepared without the organic binder using the same firing process. The denomination for these samples is P1 and P2 (see Table 1).

### 2.2. XRD

The X-ray diffraction (XRD) patterns using Siemens D5000 equipment with K$\alpha$-Cu radiation in a Bragg–Brentano geometry at room temperature (300 K), were done by step scanning using powdered samples. We used five sec for each step of counting time, with a Cu-K$\alpha$ tube at 40 kV and 25 mA.

### 2.3. Infrared Spectroscopy

The infrared spectra (IR) were measured using KBr pellets made from a mixture of powder for each glass composition. The pellet thickness varied from 0.5–0.6 mm. The IR spectra were measured from 400–1400 $cm^{-1}$ with a Nicolet 5ZPX FT-IR spectrometer.

### 2.4. Raman Spectroscopy

Micro-Raman measurements were performed using a T64000 Jobin Yvon spectrometer equipped with an $N_2$-cooled charge-coupled device (CCD) to detect the scattered light. The spectra were excited with an argon-ion laser (5145 Å). The spectrometer slits were set to give a spectral resolution of better than 2 $cm^{-1}$

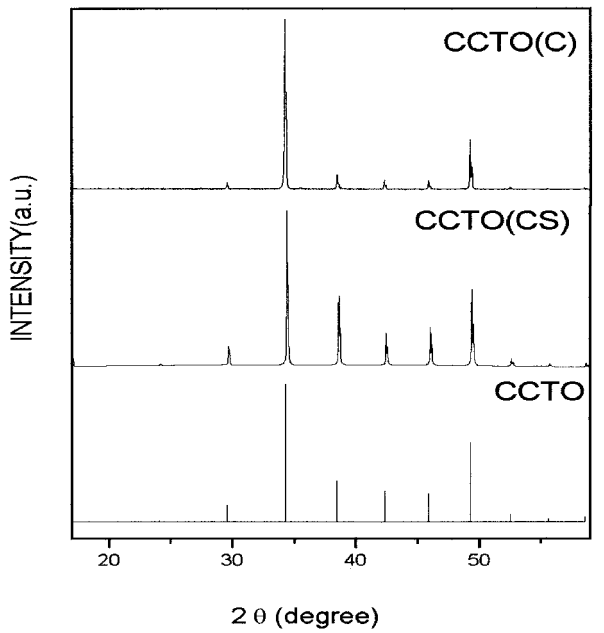


**Figure 1** Comparison of the XRD of the calcinated sample CCTO(C) and calcinated + sintered sample (CCTOCS) with CCTO reference

(always). The Raman scattering was measured by using a back-scattering geometry directly from the powder.

*2.5. Electrical Measurements*

The dielectric and loss measurements, obtained from a HP 4291A impedance analyzer, covered the region of 100 Hz to 100 MHz.

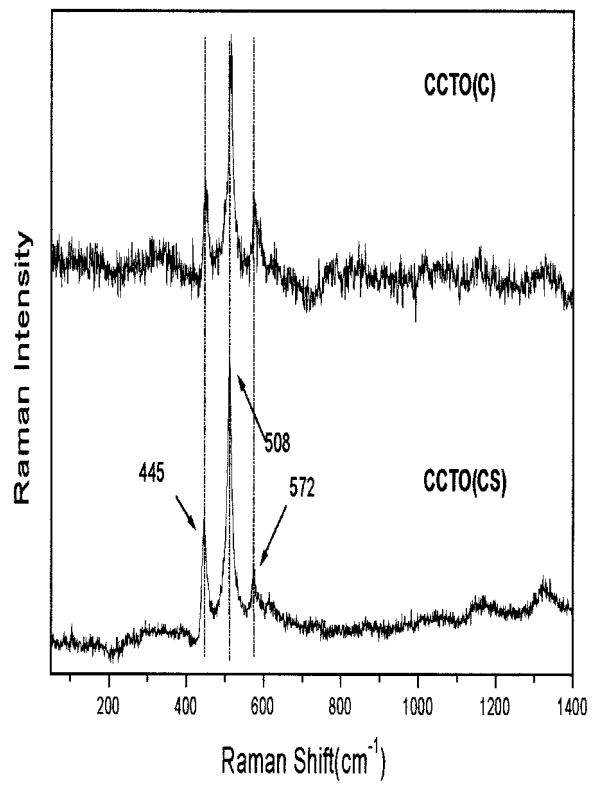


**Figure 2** Comparison of the Raman spectra of the calcinated sample CCTO(C) and calcinated + sintered sample CCTO(CS)

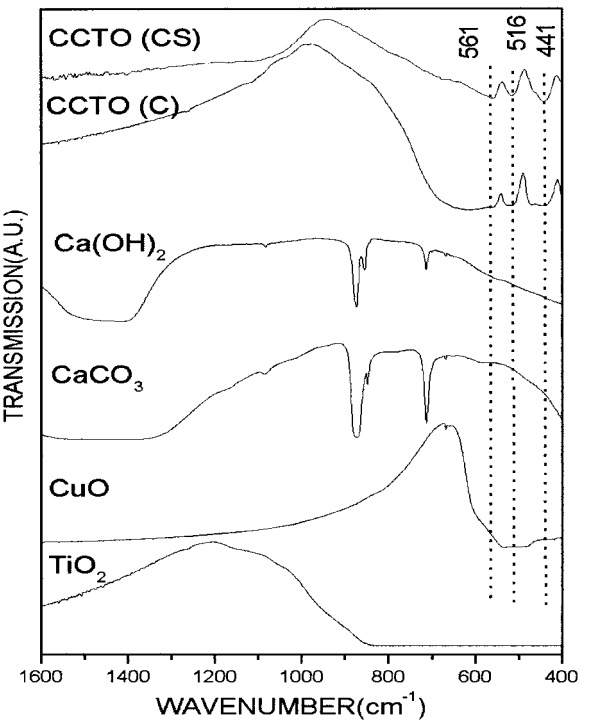


**Figure 3** Comparison of the Infrared spectra of the calcinated sample CCTO(C) and calcinated + sintered sample CCTO(CS) with the starting materials

The dielectric permittivity and loss were performed using a parallel-plate capacitor arrangement. The samples were formed into thin circular disks with a diameter of around $L = 3$ to 5 cm and thickness of around $e = 2$ mm (see Table 1). Ag circular electrodes were screen printed at each surface and fired at 400°C for 1 h.

The resonance measurements in the range of 0.3 to 3 GHz were done in a conventional setup, and the $S_{11}$ parameters were measured by using an HP 8714ET network analyzer.

## 3. RESULTS AND DISCUSSION

Figure 1 shows the XRD of the ceramic after calcinations, CCTO(C), and calcination plus sinterization, CCTO(CS). After calcination, the CCTO phase is easily identified. The posterior sintering procedure does not significantly change the diffraction pattern CCTO(CS) (see Fig. 1).

Figure 2 shows the Raman spectra of the calcined CCTO(C) and sinterized CCTO samples (CS), in which the three main peaks at 445, 508, and 572 $cm^{-1}$ are easily identified. Assignment of the Raman spectral features to the crystalline CCTO has been reported previously [2, 9]. Scattering peaks at 445, 513 and 572 $cm^{-1}$ were observed [2]. In [9] the Raman lines at 445 and 511 $cm^{-1}$ were associated with the Ag symmetry ($TiO_6$, rotationlike) and 575 $cm^{-1}$ of the Fg symmetry (O—Ti—O, anti-stretching). Agreement between the previous Raman results for CCTO with our samples obtained by the sintering process was found to be good.

Figure 3 shows the IR spectra of the ceramics CCTO(CS) and CCTO(C) together with the spectra of the starting materials. One can notice that the CCTO phase presents resonance absorptions at 561, 516, and 441 $cm^{-1}$ for CCTO(CS). Several authors have assigned [10] this region of absorptions with the titanium ion. These bands were associated to $\nu_{Ti—O} = 653–550$ $cm^{-1}$ and $\nu_{Ti—O—Ti} = 495–436$ $cm^{-1}$.

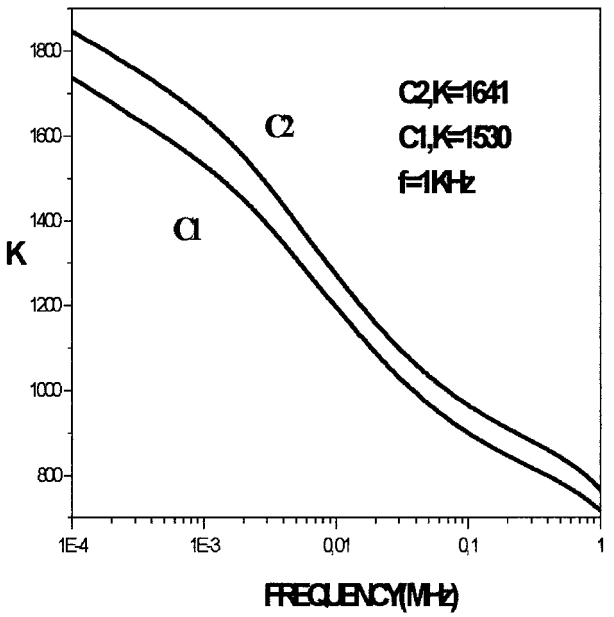


**Figure 4** Dielectric constant $K$ of samples C1 and C2 in the frequency range of 100 Hz to 1 MHz

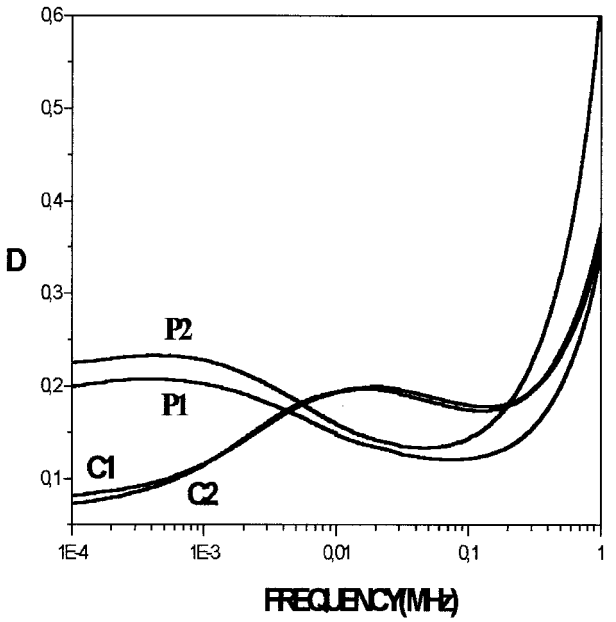


**Figure 6** Dielectric loss ($D = tg\alpha$) of samples C1, C2, P1, and P2 in the frequency range of 100 Hz to 1 MHz

Figures 4 and 5 show the dielectric permittivity ($K$) of all the samples (C1 and C2 in Fig. 4 and P1 and P2 in Fig. 5) in the range of 100 Hz to 1 MHz. For all the samples, there is a decrease in the $K$ value for this range of frequency. For samples C1 and C2 at 100 Hz, $K \sim 1800$ decreases to 800 at 1 MHz. For samples P1 and P2, where we did not use any organic binder, the dielectric constant was higher. For samples P1 and P2 at 100 Hz, $K \sim 10.000$ decreases to 4.000 at 1 MHz. We believe that the presence of the organic binder plays a critical role in its effect on the grain size and boundaries, which thus affects the effective dielectric constant of the ceramic [8]. Figure 6 depicts the dielectric loss for all the samples. At low frequencies, the P1 and P2 samples present higher losses, as compared to the C1 and C2 samples. The loss increases with the frequency and is around 0.35 for samples C1 and C2 at around 1 Mz. Table 1 gives the dielectric constant and loss for all the samples at 1 KHz and 1 MHz.

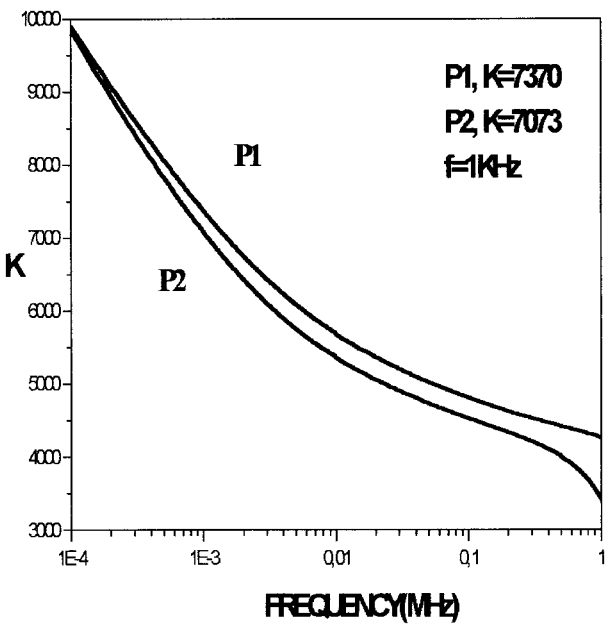


**Figure 5** Dielectric constant $K$ of samples P1 and P2 in the frequency range of 100 Hz to 1 MHz

The increase of the loss for all the samples with frequency has been reported in the literature [8].

To investigate the potential application of the CCTO materials for microwave planar devices, a series of planar microstrip antennas was made. The demand for new mobile communication systems will lean heavily toward miniaturization and low-volume devices and equipment. Due to these requirements in portable or repeater stations in cellular systems for mobile communication for example, high dielectric constant materials can be used to effectively reduce the size of planar microstrip antennas [11].

The performance of a planar antenna is related to the $L$ and $W$ dimensions of the patch and the dielectric constant $K$ of the substrate. For the best compromise among antenna gain, efficiency, bandwidth, and volume, an adequate material with a high $K$ must be found for low volume. Of course, there is a tradeoff: high dielectric constant materials provide a low-volume antenna, but impose low bandwidth and gain. Moreover, there is a demand for monolithic integration of antennas and associated circuitry and these requirements claim compatible high dielectric constant materials.

Simple rectangular antenna prototypes were designed on substrate samples nominally 3–4 cm in diameter and 2–3 mm thick (see Table 1). The resonant frequency was calculated in the range of 2–3 GHz, based on the dielectric constant available data [1–3, 8]. One of the experimental antennas is shown in Figure 7 (sample C1).

All the samples show the electromagnetic radiator's potential properties, that is, antenna. This is proved when the dips in the $S_{11}$ measurements reach values lower than $-10$ dB. The $-10$-dB point in the $S_{11}$ parameter corresponds to a VSWR of 2:1. The $S_{11}$ parameters (return loss) for the antennas were measured. The results are shown in Figure 8 for the P1 antenna. The VSWR $< 2{:}1$ ($-10$-dB line) criterion, used to identify the antenna bandwidth and the dip in the $S_{11}$ measurement (see Fig. 8) below $-10$ dB, is

a preliminary indicator of the electromagnetic radiation properties of the device.

As a typical result, a 90-MHz BW was found for the antennas (with P2, C1, and C2 as substrates), which is lower than that of typical rectangular patch antennas with low dielectric constant substrates, of about 3%. The antenna with P1 substrate presented a surprisingly high BW of 270 MHz that corresponds to 10% bandwidth at 3 GHz. Such a value is in accordance with the requirements for planar antennas in a variety of wireless communication systems, such as WLAN, PCS, Wi-Fi, and other protocols. Therefore, these measurements confirm the potential use of such materials for small planar high dielectric antennas (HDA).

In summary, the CCTO samples present higher DC for the samples prepared without any organic binder ($K = 7370$ and 7073 for P1 and P2, respectively, at 1 KHz), as compared to the samples prepared with the organic phase ($K = 1641$ and 1530 for C2 and C1, respectively, at 1 KHz); refer to Figures 4 and 5 and Table 1. The presence of the organic phase can be used to control the value of the DC and loss of the material. However, the loss is still a problem to be studied regarding applications in the microwave region.

The performance of a planar microstrip antenna that uses the CCTO ceramic as a high DC substrate was examined. Simple rectangular antenna prototypes were designed on substrate samples (C1, C2, P1, and P2; see Table 1). For the antennas (with P2, C1, and C2 as substrates), the BW is 90 MHz (around 3%). The antenna with P1 substrate presented a surprisingly high BW of 270 MHz that corresponds to a 10% bandwidth at 3 GHz. Such a value is in accordance with the requirements for planar antennas for a variety of wireless communication systems such as WLAN, PCS, Wi-Fi, and other protocols. Therefore, these measurements confirm the potential use of such materials for small high-dielectric planar antennas (HDA).

These materials are also very promising for capacitor applications and certainly for microelectronics and microwave devices (cellular mobile phones, for example), where miniaturization of the devices is critical.

## 4. CONCLUSION

In conclusion, a traditional ceramic (solid-state) procedure was used to produce bulk ceramics of CCTO ($CaCu_3Ti_4O_{12}$). The samples of the CCTO ceramic were studied by X-ray powder diffraction, and infrared and Raman scattering spectroscopy. After 30 h of milling, the formation of CCTO was confirmed by X-ray powder diffraction. The infrared and Raman scattering spectroscopy confirmed the formation of the CCTO phase as seen by XRD analysis. The first experimental procedure used an organic binder in the process of shaping the samples. In the second procedure, the samples were prepared without the presence of the organic phase, and we obtained a higher dielectric constant ($K = 7370$) with high loss ($D = 0.2$) at 1 KHz. For the first procedure, a lower dielectric constant ($K = 1530$) and lower loss ($D = 0.11$) at 1 KHz were obtained. Simple rectangular antenna prototypes were also designed on substrate samples (C1, C2, P1, and P2). For the antennas (with P2, C1, and C2 as substrates), the BW was 90 MHz (around 3%). The antenna with P1 substrate presented a surprisingly high BW of 270 MHz, which corresponds to a 10% bandwidth at 3 GHz. Such a value is in accordance with the requirements for planar antennas in a variety of wireless communication systems, such as WLAN, PCS, Wi-Fi, and other protocols. Therefore, these measurements confirm the potential use of such materials for small planar antennas. These materials are attractive for capacitor applications, as well as for microelectronics and microwave devices (cellular mobile phones, for example), where miniaturization of the devices is crucial.

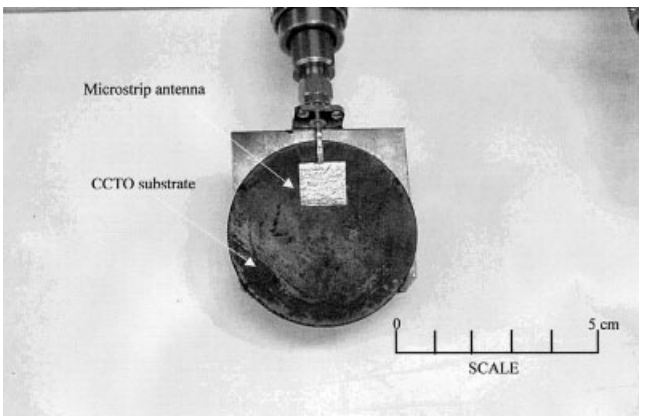


**Figure 7** Planar microstrip antenna on CCTO substrate for 3-GHz operation

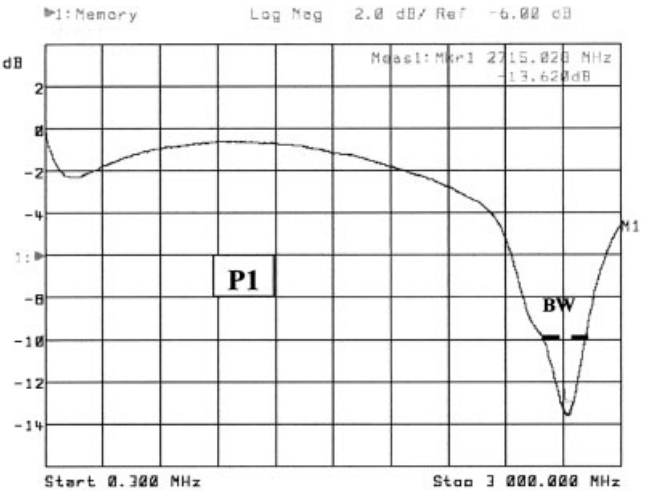


**Figure 8** Resonant frequency of the microstrip antenna of sample P1, measured through the $S_{11}$ parameter (return loss). The BW is obtained at $-10$ dB, which corresponds to VSWR $< 2:1$


## ACKNOWLEDGMENTS

This work was partly sponsored by Ericsson EDB, Ericsson Research Center Brazil, under contracts Ericsson/UFC-06 and UNI.15/00 and by FINEP, CNPq, CAPES (Brazilian agencies). We also thank A. G. Souza Filho for the Raman measurements.


## REFERENCES


1. M.A. Subramanian, D. Li, N. Duran, B.A. Reisner, and A.W. Sleight, J Solid State Chem 151 (2000), 323–325.
2. A.P. Ramirez, M.A. Subramanian, M. Gardel, G. Blumberg, D. Li, T. Vogt, and S.M. Shapiro, Solid State Commun 115 (2000), 217.
3. M.A. Subramanian and A.W. Sleight, Solid State Sci 4 (2002), 347.
4. N. Setter and E.L. Colla, Ferroelectric ceramics, Birkhauser Verlag, 1993.
5. B. Bochu, M.N. Deschizeaux, and J.C. Joubert, J Solid State Chem 29 (1979), 291.
6. A.F.L. Almeida, R.S. de Oliveira, J.C. Góes, J.M. Sasaki, J. Mendes Filho, and A.S.B. Sombra, Mat Sci and Eng B 96 (2002), 275–283.
7. R.S. de Figueiredo, A. Messai, A.C. Hernandes, and A.S.B. Sombra, J Mat Sci Lett 17 (1998), 449.
8. P. Jha, P. Arora, and A.K. Ganguli, Mat Lett 4179 (2002), 1–4.

9. N. Kolev, R.P. Bontchev, A.J. Jacobson, V.N. Popov, V.G. Hadjiev, A.P. Litvinchuk, and M.N. Iliev, Phys Rev B 66 (2002), 132102.
10. S. Music, M. Gotic, M. Ivanda, S. Popovic, A. Turkovic, R. Trojko, A. Sekulic, and K. Furic, Mat Sci and Eng B 47 (1997), 33.
11. B. Lee and F.J. Harackiewicz, IEEE Trans Antennas Propagat 50 (2002), 1160.



# A NEW COMPACT 1D PBG MICROSTRIP STRUCTURE WITH WIDER STOPBAND BASED ON SEMICONDUCTOR SUBSTRATE

**Wenmei Zhang,[1,2] Xiaowei Sun,[2] Junfa Mao,[1] Rong Qian,[2] and Dan Zhang[2]**
[1] Department of Electronic Engineering
Shanghai Jiao Tong University
Shanghai, 200030, P. R. China
[2] Shanghai Institute of Micro-system and Information Technology
Chinese Academy of Sciences
Shanghai, 200050, P. R. China

*Received 26 March 2003*

**ABSTRACT:** *A new type of compact one dimensional (1D) microstrip photonic bandgap (PBG) used for filters is presented. A semiconductor-based structure of a miniature band-stop filter with three cells is simulated, realized, and measured. Basic agreement between the experimental and simulated results have been achieved. The filter with the proposed PBG structure exhibits wide, deep, and steep stop-band characteristics, and also has less loss and ripples in the pass-band. Thus, the new PBG structure can be used for low-pass as well as high-pass filters. The period of the PBG lattice is about (1/5 ~ 1/4) $\lambda_e$ ($\lambda_e$ is the guiding wavelength at the center frequency of the stop-band), or 0.08 $\lambda_0$ ($\lambda_0$ is the wavelength in air). The filter with the new PBG structure is much easier to fabricate and integrate with other circuits and is more compact than conventional filters. The results in our paper are based on semiconductor substrate and can be applied directly in MIC and MMIC.* © 2003 Wiley Periodicals, Inc. Microwave Opt Technol Lett 39: 150–152, 2003; Published online in Wiley InterScience (www.interscience.wiley.com). DOI 10.1002/mop.11153

**Key words:** *microstrip; photonic bandgap (PBG); bandstop filter; low-pass filter; high-pass filter; slow wave*

## 1. INTRODUCTION

The idea of employing photonic bandgap (PBG) was first proposed by Yabnolovitch in 1987 [1]. A PBG device is a periodic structure in which electromagnetic waves in a certain frequency band cannot propagate or be strongly attenuated. Therefore, it has been used largely for electromagnetic wave propagation control. Also, a PBG device is slow-wave structure. When it was introduced, the size of devices can be reduced.

Several papers have focused on achieving compact design and wider frequency stopband. For example, Kelly [2] proposed a serial connection of several different PBG structures for wide-rejection-frequency bandwidth, but this required large size and had limitations for microstrip-circuit applications of compact size. In [3], the proposed structure was connected in parallel with two periodic structures that have different center frequencies of the stopband. In [4], a novel multiplayer structure was used to enhance the width of the stopband. The abovementioned filters have etching in the ground plane. A disadvantage of this structure is packaging problem and realization of MMICs: the etched ground plane must be sufficiently far from any metal plate in order to maintain the etched patterns' function. Also, the position of the signal line in reference to the etched ground plane has an influence on the final characteristics. So, Nesic proposed a novel PBG microstrip structure without etching in the ground plane as a filter [5], which is also a low-pass filter.

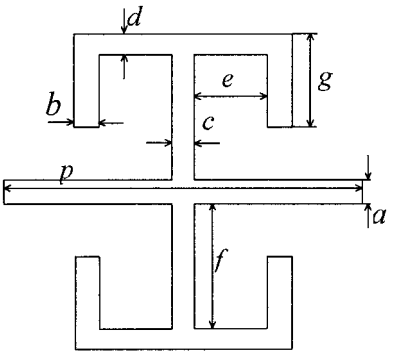


**Figure 1** Proposed 1D microstrip PBG cell

In this paper, a new compact microstrip PBG structure for filters is proposed. The filters adopting the proposed PBG structure exhibit wide, deep, and steep stop-band characteristics, and also have small and few ripples at the higher pass-band. So it can also be used in high pass filters. The period of the PBG lattice is about (1/5 ~ 1/4) $\lambda_e$. The simulation was done using Agilent ADS software.

## 2. DESIGN OF THE NEW 1D MICROSTRIP PBG CELL

The proposed 1D microstrip PBG cell is shown in Figure 1. Inductance corresponds to the narrow lines, and capacitance corresponds to the gap between the narrow lines (Fig. 1). The additional capacitance and inductance determine the propagation constant, which is much larger than that of a conventional microstrip line. The achieved slow-wave can be used to reduce the size of filter. By tuning the length of every line and the gap between the lines, different slow-wave effects can be attained at different frequency. For simple design, $a = b = c = d$ is assumed.

## 3. MEASUREMENT RESULTS

According to the characteristic of the proposed PBG structure, a filter with wider stopband for a system is designed. The signal of the system comes from the oscillatory working at 16.5 GHz. This filter was originally developed to meet the following specifications for a system application.

| | | |
|---|---|---|
| Min. stop-band rejection: | 16.5 GHz | −20 dB |
| | 33 GHz | −10 dB |
| Insertion loss: | 36 GHz | −2 dB |

The realized filter is shown in Figure 2. The substrate used is gallium-arsenide with a dielectric constant of 12.6 and thickness of 0.25 mm. The $S$ parameter was measured with an HP 8722D net analyzer and a Casecade probe station. The simulated and measured $S$ parameters for $a = b = c = d = 0.09$ mm, $e = 0.14$ mm, $f = 0.53$ mm, $g = 0.44$ mm, and $p = 0.94$ mm are shown in Figure 3. The phase responses of the realized structure (including the 50Ω microstrip line for connectors) and a 50Ω microstrip line of the same length are presented in Figure 4. In Figure 3, basic agreement between the experimental and simulated results has